TOWARDS A HIGH-PACKING-RATIO LINEAR ACTUATOR FOR USE IN CABLE DRIVEN PARALLEL MANIPULATORS

Andrew C. Mathis[1], Juan Antonio Carretero[1], Yves Losier[1]
[1]*Department of Mechanical Engineering, University of New Brunswick, Fredericton, NB, Canada*
Email: juan.carretero@unb.ca

ABSTRACT

The workspace of cable-driven parallel manipulators (CDPMs) and the forces they can apply are limited by the fact that cables cannot support compressive loads. Linear actuators that can support compressive loads, but have the benefits of cables could be used to build hybrid CDPMs. In this work, designs using three sections of a retractable metal tape measure for the extended portion, or beam, of an actuator are studied. Different methods to keep the three sections together are studied, including strip magnets. Prototype beams were tested in compression and bending, and the impact of varying the strip magnet and tape measure widths were explored as well as adding a spring core. The effects of inertia and acceleration on tip displacement during dynamic loading were also investigated. A strip magnet with an external brace design had the highest loading capacities, which increased as tape width increased. During dynamic testing, higher accelerations caused higher tip deflections. Future work is needed to design and build an actuator using this beam design.

Keywords: linear actuator; high-packing-ratio actuator; cable-driven parallel manipulator.

ACTIONEUR LINÉAIRE À GRAND RAPPORT D'EMBALLAGE POUR DES MANIPULATEURS PARALLÈLES ENTRAÎNÉS PAS DES CÂBLES

RÉSUMÉ

L'espace de travail des manipulateurs parallèles entraînés par des câbles (CDPM) et les forces qu'ils peuvent appliquer sont limités par le fait que les câbles ne peuvent pas supporter des charges de compression. Des actionneurs linéaires capables de supporter des charges de compression, mais bénéficiant des avantages des câbles, pourraient être utilisés pour construire des CDPM hybrides. Dans ce travail, des conceptions utilisant trois sections de ruban à mesurer en lame incurvées d'acier pour créer une poutre de section triangulaire et de longeur variable sont étudiées. Differentes façons de ratacher les trois rubans sont etudiées. Les differentes poutres prototypes ont été testées en compression et en flexion. L'impact de la variation de la largeur des bandes magnétiques et du ruban a été étudié, de même que l'ajout d'un noyau de ressort sur toute la longeur de la poutre. Les effets de l'inertie et de l'accélération sur le déplacement de la pointe lors de l'application des forces dynamiques ont également été étudiés. Les poutres avec une conception contenant des pièces de soutien externes avaient les capacités de charge les plus élevées, qui augmentaient avec la largeur du ruban. Au cours des tests dynamiques, des accélérations plus élevées ont provoqué des déviations plus élevées de la pointe de la poutre. Des travaux futurs sont nécessaires pour concevoir et construire un actionneur utilisant cette conception de poutre avec des rubans à mesurer.

Mots-clés : actioneur linéaire ; actioneur avec un grand rapport d'emballage ; manipulateurs parallèles entraînés par des câbles.

1. INTRODUCTION

As a subset of parallel manipulators (PMs), cable driven parallel manipulators (CDPMs), use a system of winch-driven cables on pulleys to position and orient (together referred to as pose) an end effector. An example of such a system is the SkyCam invented by Garrett Brown [1], which uses four cables to support a camera over stadiums to get overhead shots of sports games and other events.

There are multiple benefits and limitations to using cables as actuators in PMs. Cables are simple, can have high loading capacities, are light and therefore can be used in high speed applications, and also have very high-packing-ratios; long lengths of cable can be efficiently stored on a relatively small spool. The downside is that cables can only support unidirectional tensile loads (*i.e.*, a cable can only pull). This key limitation restricts the workspace of CDPMs. To keep cables in tension, either gravity must be depended on as in the case of the SkyCam, or complementary cables must be added to allow forces to be applied in opposing (antagonistic) directions. Since the cables cannot push, the pulleys create a bounding volume of the maximum theoretical reachable workspace of the manipulator.

As a subset of the reachable workspace, the wrench workspace is the region where the PM can apply or sustain a specified minimum force/moment couple, together referred to as wrench, in any direction [2]. This is important to understand during the synthesis of a PM to ensure that the force requirements of its intended tasks are achievable in the areas of the workspace where the tasks are to be performed. Additionally, since CDPMs are redundantly actuated, that is that they have more actuators than their degrees of freedom, some poses can be sustained by any one of an infinite number of sets of cable forces. In order to solve this problem, the force capabilities of CDPMs can be analyzed using polytopes; flat-sided geometric objects.

As shown in [2], one measure of the force capability of a CDPM at a given pose uses six-dimensional polytopes. This is done by mapping the extreme force/moment limits of the actuators to a polytope of wrenches that they can create at the end effector in the task space [3]. One can then measure the radius of the largest origin-centred sphere the polytope can contain. This radius is the minimum wrench capability of the manipulator at that pose.

Due to CDPMs not being symmetrically actuated, the actuators can only apply tensile forces, the wrench capabilities of the manipulator at any point are not necessarily centred at the origin of the task space. If there were some way for the cables to apply both compressive and tensile forces (*i.e.* more symmetrically actuated), there would be more of a range of forces available at the actuator, resulting in increased minimum wrench capabilities and a higher quality workspace.

1.1. Problem Statement

To address the workspace size and quality limitations of CDPMs, a linear actuator may be used which can both pull and push while retaining the cable's property of having a high-packing-ratio to replace at least one cable in a CDPM. Since such an actuator could sustain compressive loads, it could push the end effector outside of the bounded volume, creating hybrid (cable and linear actuator) CDPMs with a much greater workspace than similar non-hybrid CDPMs. With the manipulator being more symmetrically actuated, the quality of the workspace will improve as well, increasing the wrench workspace even within the original reachable workspace. With the hybrid CDPM's workspace no longer bounded by the pulleys but by the new actuator's extension length, the manipulator's footprint and/or number of actuators could be reduced.

As this actuator's maximum loading capacity will decrease with length, it will not be feasible for large scale CDPM applications such as the SkyCam. Instead, this actuator would be well suited for mechanisms with workspaces in the region of 1 m^3, as it is expected that loading capacity of the actuator will decrease to a point where it is no longer practical at longer lengths. Applications with workspaces in this range include pick-and-place PMs, and therefore the long-term goal of this work is to create hybrid CDPMs with these high-packing-ratio linear actuators for use in high speed pick-and-place PMs.

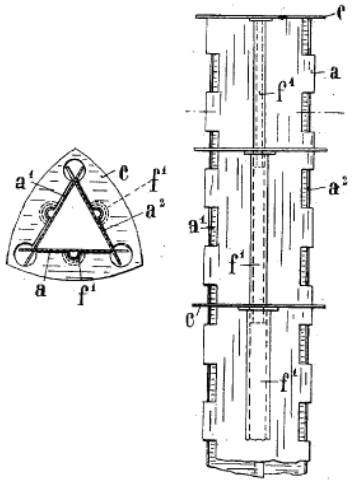

Fig. 1. Portable extensible and retractable mast patent [5] by Jaeger and Siewert.

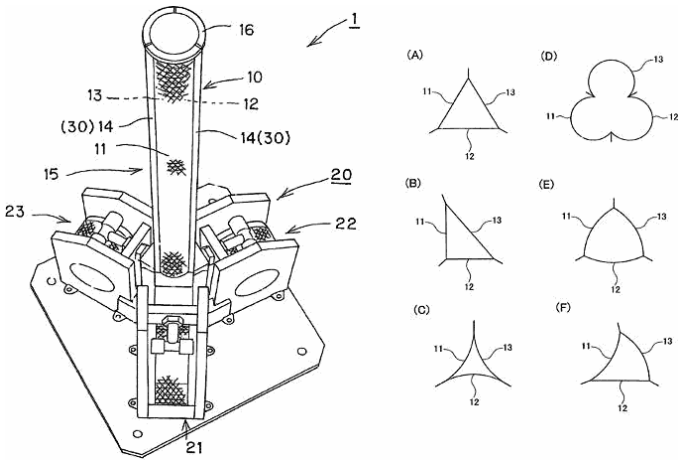

Fig. 2. Extendible structure patent by Watanabe *et al.* [6].

1.2. Objectives

The objective of this work is to study the feasibility of a high-packing-ratio linear actuator and understand its maximum force capabilities. First, existing high-packing-ratio linear actuators were investigated to understand the current state of the art. Next, different prototypes beams were built that could be used in a high-packing-ratio linear actuator, and they're maximum loading capacities in compression and bending were tested. These experimental results were compared with theoretical calculations, and then a single beam type was tested in a simple hybrid CDPM and its performance was measured during dynamic tests.

1.3. Literature Review

A review of existing technologies was performed in order to understand the current state of the art. A similar review of existing deployable boom technologies was performed by NASA in 1976 [4] for application to deploying solar cell arrays in orbit. These comprehensive reviews compared many different technologies including folding trusses, rigid chain actuators, rigid belt actuators, segmented spindle actuators, and thin-walled tubular booms. Of these high-packing-ratio linear actuators, the thin-walled tubular booms were chosen as most promising due to their low weight and very high-packing ability. Of the types of thin-walled tubular booms that were investigated, the most relevant type is close-section triangular booms. The idea with close-section triangular booms is to have three seperate sides in a retracted (often coiled) form that can be deployed, as well as a method to hold the three sides together. Triangular boom concepts go back to 1910 and patents have been issued as recently as 2014 [5, 6]. More details on this review can be found in [7].

In 1910, Jaeger and Siewert presented an extensible mast whose edges interlock and are held together by periodic cross braces as seen in Figure 1 [5]. These cross braces are engaged by protrusions on the mast's sides that start small and get wider. Watanabe *et al.* [6] patented an extendible structure with three sides, but show the actuator and 6 possible boom cross sections, as shown in Figure 2. Watanabe *et al.* list hook-and-loop fasteners as the preferable method of attaching the sides, but also include "line fasteners, rail fasteners, magnets, latches, hooks, buttons, adhesion, and bonding" in their patent.

Although the elastic buckling characteristics of thin-walled straight triangular members has been studied, no research on closed curved triangular sections has been found by the author to this date. In the present work, the attachment methods for closed-section triangular booms were investigated, specifically closed-section triangular booms made using steel tape measure sections.

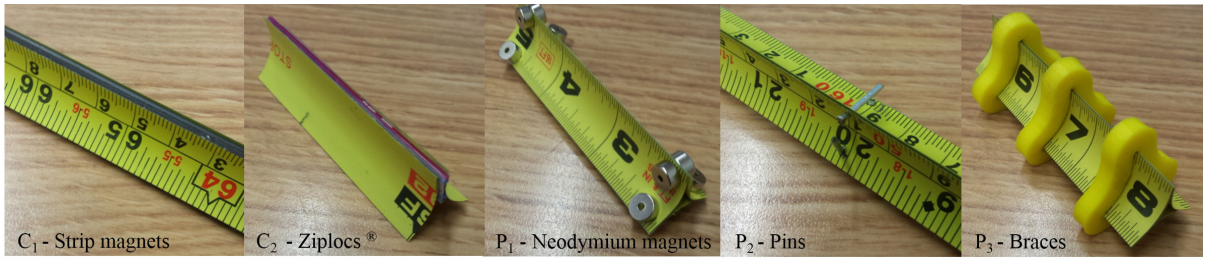

Fig. 3. Attachment methods considered.

2. QUASI-STATIC TESTING

In order to understand the force capabilities of a high-packing-ratio linear actuator, quasi-static testing of sample beams was performed. The testing is quasi-static as although the beam is moving through the test, the loads are being applied so slowly that inertial effects can be disregarded and the beam deforms in a static manner. These experimental results were then compared to results determined analytically.

The scope of beam designs was limited to closed cross section triangular beams composed of steel tapes with different methods of attaching the tapes. Testing was done to determine the effect of various attachment methods on the maximum loading the beam could withstand in compression and bending. After this, the best attachment option was selected as the beam design for the remainder of the work and some refinement of the chosen design was performed to reduce its mass. Finally, the effect of varying the tape width as well as the effect that a centre supporting spring had on the maximum loading of a single beam design was determined in compression and bending.

2.1. Tape Attachment Methods

Several attachment methods for connecting the sides of a triangular boom have been presented in the literature, including hook-and-loop fasteners, magnets, holes and protrusions, zippers, and cross sectional braces. Due to the limited cycle life of hook-and-loop fasteners, they were considered unsuitable for the high speed cyclic application of a CDPM linear actuator. For this work, two types of magnets were considered (strip and neodymium), as well as Ziplocs®, pins, and braces, as shown in Figure 3. The strip magnets are flexible and have an adhesive backing that was used to fix them to the steel tape sections, and the neodymium magnets were held in place by another magnet on the opposite side of the tapes. The Ziplocs® were cut from Ziplocs® bags and super-glued between the tapes, the pins were inserted through holes drilled in the tapes, and the braces were 3D printed to match the geometry of the beams. These attachment methods were assigned codes as shown in Figure 3, and divided into two categories: continuous (C) and periodic (P).

Combining one periodic and one continuous method creates 12 possible options, as can be seen in Table 1, where C_0 and P_0 represent a lack of continuous and periodic attachments respectively in that option. The C_0P_0 involves no attachments between the tapes, and is included in the testing as a baseline of how the tapes behave without constraints.

As this is a feasibility study, the general effects of each of these attachment combinations is being investigated, and as such only single designs of each are to be tested. For instance, only a single type of pin, brace design, or spacing of the periodic attachment methods will be tested. A common spacing of the periodic attachment methods was arbitrarily chosen as 10 cm.

2.2. Apparatuses

In order to measure the maximum compressive force and bending moment of each type of beam, jigs were fabricated such that all of the testing was performed on a universal testing machine (UTM). UTMs allow samples to be loaded in various configurations while the applied force and deflection are recorded.

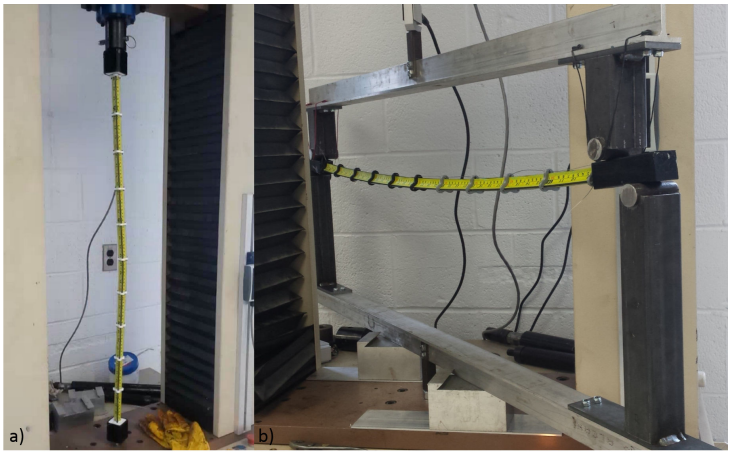

Fig. 4. Compression (a) and bending (b) testing.

Table 1. Attachment options / combinations.

	P_0	P_1	P_2	P_3
C_0	C_0P_0	C_0P_1	C_0P_2	C_0P_3
C_1	C_1P_0	C_1P_1	C_1P_2	C_1P_3
C_2	C_2P_0	C_2P_1	C_2P_2	C_2P_3

Table 2. Summary of quasi-static experiments.

Factor of interest	Attachment methods	Magnet widths	Tape widths widths	Spring core
Attachments	13	1	1	No
Magnet width	1	2	1	No
Tape width	1	1	3	No
Spring core	1	1	1	Yes/No

In order to perform compression testing on the UTM, a jig was created to hold the beam's ends in place, with both ends fixed. Although these boundary conditions do not reflect the expected conditions in the CDPM application, they were necessary to make the results reflect only the beam and not the 3D printed extensions. Figure 4a shows a beam in the compression jig undergoing a compression test in the UTM. This jig fits over extensions on the ends of the beams, which were 3D printed such that the ends of the beam are straight and held rigidly in place by being encased in resin.

A four-point bending jig was created for the bending testing as shown in Figure 4b. This jig allows equal moments to be applied at each end of the member such that the free length of the member experiences a uniform moment. These moments will be applied to 10 cm extensions added to the ends of the members so that the moment is applied evenly and without changes in cross sectional area at the ends.

2.3. Experiments

In order to investigate the effects of the attachment options, magnet width, tape width, and spring core on the maximum loading capacity of the beams, a series of four experiments were conducted twice, once in compression and once in bending. These experiments are outlined in Table 2. With a sample size of 3, a total of 90 samples were created for quasi-static testing.

To reduce the number of samples, not all of the attachment options were tested in each loading condition. Since the main purpose of the actuator in the CDPM application is to apply and sustain axial forces, compressive testing was performed first and with all 13 attachment methods. Next, the top 6 attachment options that performed best in compression were selected for bending testing, along with the C_0P_0 attachment option for a total of 7. Finally, the best option was selected for the remainder of the research. Using this selected beam design, the impacts of varying the width of the strip magnets and the steel tape were studied. Magnet widths of 2.08 and 3.13 mm, and tape widths of 12.70, 19.05, and 25.40 mm were used.

Table 3. Average compression test results for attachment options, in N.

	P_0	P_1	P_2	P_3	Avg.
C_0	36	176	233	219	166
C_1	420	401	321	509	413
C_2	289	342	359	276	317
Avg.	248	306	304	335	298

Table 4. Average bending test data for the attachment options, in Nm.

	P_0	P_1	P_2	P_3	Avg.
C_0	0.6				0.6
C_1	4.5		4.7	5.1	4.7
C_2	4.0	3.7	3.8		3.9
Avg.	3.0	3.7	4.2	5.1	3.6

A portion of the failure of these beams was expected to be when the steel tapes buckle inward. An idea to reduce this effect was to insert a support inside of the curved triangular space formed by the three tapes. In order for this support to also have a high-packing-ratio, it must also be able to coil, so a compression spring was chosen as it can coil, support the required loads, and its density can be varied with its pitch. The size of the compression spring was selected to just contact the middle each tape.

2.4. Results

The average results from testing the effect of the attachment options on the loading capacity of samples in compression can be seen in Table 3, where the attachment option with the highest average compressive loading capacity was C_1P_3. As can be seen in these results, the continuous and periodic attachment methods that contributed the most to the compression strength of the beams were C_1, or the strip magnets, and P_3, or the braces, respectively. Also, as expected, the two null options had the worst performance. C_1 was found to be significantly higher than C_2 and C_0, and P_1 and P_3 were found to be significantly higher than P_0.

For the experiment to determine the effect of the attachment options on the loading capacity of beams in bending, it was previously determined that the 6 highest performing beam types would be selected for further bending testing along with the C_0P_0 option. After seeing the compression results, it was decided that C_1P_1 would be removed from this list allowing the 7th highest beam type, C_2P_0, on to the bending testing. This was due to the fact that C_1P_1 was found to be nearly identical in strength to C_1P_0 even though neodymium magnets had been added. It was hypothesized that the neodymium magnets had very little impact on the beam's performance due to the other magnetic material in between them, and the 4 mm gap between the magnets. The average data collected from the bending tests can be seen in Table 4. Similar to the results from the compression testing, C_1 (the strip magnets) and P_3 (the braces) contributed the most to the bending strength of the beams, and the two null options had the worst performance. The only major difference between these main effects and the compression main effects is that P_2 (the pins) had more of an impact on the bending strength than the compression strength.

With the attachment method testing in compression and bending completed, the C_1P_3 beam option was selected as the beam type for the remainder of this work. This was due to it having the best performance in both compression and bending, and a below-average unit cost of the beam types tested. The only drawback with this beam type is its mass, at 397.7 g/m. In order to reduce this mass, a stronger strip magnet material was used which allowed lighter beams to be created.

The results of the magnet width testing in compression and bending can be seen in Table 5. Here, increasing the magnet width was found to decrease the maximum loading capacity in compression, and only slightly increase it in bending. One possible reason for the decrease in compressive loading capacity with a larger magnet width could be due to the beam's cross section. With the curved triangular shape, the tapes are only parallel at their edges, and from there the distance between them increases. Wider magnets have edges that are further apart, and this initial gap can significantly reduce their strength.

The effect of different tape widths on the maximum loading of the beams in compression and bending was investigated using only the C_1P_3 attachment option with the average results as seen in Table 6. Overall,

Table 5. Magnet width testing average results.

Width (mm)	Compression (N)	Bending (Nm)
2.08	460	4.5
3.13	301	4.8

Table 6. Tape width testing average results.

Width (mm)	Compression (N)	Bending (Nm)
12.70	162	1.9
19.05	301	4.8
25.40	420	5.1

Table 7. Spring core testing average results.

Spring core	Compression (N)	Bending (Nm)
0	301	4.8
1	321	5.1

the compressive strength of the beams can increases in a near linear manner as the tape width increases. In bending, the effect of increasing the tape width also increases the beam strength. However, the increase from the 19.05 mm tape to the 25.40 mm tape is much less than the increase from 12.70 mm to 19.05 mm.

The average results of the spring core testing in compression and bending can be seen in Table 7. Here, it is clear that there was minimal improvement in either the compressive or bending strength of the beam by adding the spring core.

Summarizing the quasi-static testing, C_1P_3 was found to have the maximum loading capacity in both compression and bending. Increasing the magnet with was found to slightly increase the maximum loading capacity in bending, but decreased the capacity in compression. Increasing the tape width significantly increased the loading capacities in compression and bending, while adding a spring core had little impact.

2.5. Comparison to theoretical calculations

Theoretical critical loads and moments were estimated to compare with the beams of each continuous attachment method. The impacts of the periodic attachment methods were ignored, and only the spacing between the edges of the tapes due to the continuous method was used; 0 mm for the C_0P_X case, 3 mm for the C_1P_X case, and 4 mm for the C_2P_X case. In the C_0P_0 case with the three constituent tapes being separate, buckling was calculated at 3 times the critical buckling load of a single tape.

2.5.1. Buckling theory

A member in compression can buckle through three different modes: flexural, torsion, and flexural-torsional buckling [8]. The common flexural buckling occurs when a column deflects laterally under a compressive load. Torsional buckling manifests as a rotation about the member's longitudinal axis and only occurs in compression members that have doubly symmetric cross sections with thin sections. Finally, flexural-torsional buckling occurs as a combination of the previous two types, a twisting with lateral deflection, and only occurs in members with only one axis of symmetry and is therefore not applicable to the current design. Of the buckling modes that apply to a particular cross section, the one with the lowest critical load will be the mode in which the member fails.

The critical load at which flexural buckling of a column occurs is a function of the column's slenderness ratio, which is the ratio of the effective length, L_e, to the radius of gyration, r. The effective length is the unsupported length multiplied by an effective length factor that represents the end conditions of the column. At high slenderness ratios, Euler elastic buckling determines the critical load ($P_{cr.Euler}$) and the critical torsional buckling load ($P_{cr.\phi}$) as

$$P_{cr.Euler} = \frac{\pi^2 EA}{\left(\frac{L_e}{r}\right)^2} \quad \text{and} \quad P_{cr.\phi} = \frac{1}{r_o^2}\left(GC_t + \frac{EC_w\pi^2}{L_e^2}\right) \tag{1}$$

where r_o is the polar radius of gyration, G is the shear modulus, C_t is the torsional constant, and C_w is the warping constant [9].

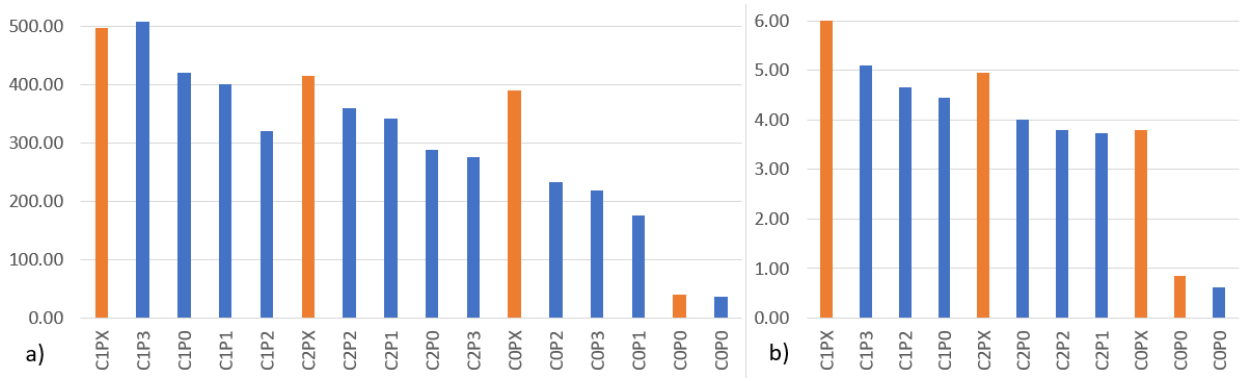

Fig. 5. Theoretical and experimental buckling loads; a) compression results in N, b) bending results in Nm.

For thin-walled members in bending with low torsional and warping stiffnesses, lateral torsional buckling can occur at the critical moment

$$M_{cr} = \frac{\pi^2 EI}{(Lk_z)^2}\sqrt{\left(\frac{k_z}{k_w}\right)^2 \frac{C_w}{I} + \frac{(Lk_z)^2 GC_t}{\pi^2 EI}} \tag{2}$$

where the constant k_w is 1 if the beam's cross section is allowed to warp at its ends, and 0.5 if warping is constrained, and likewise k_z is 1 if the beam is allowed to deflect laterally at its ends and 0.5 if it is constrained [10].

2.5.2. Compression and bending results

The results for these theoretical values are compared to the experimental data in Figure 5a, where the bars in orange are the theoretical values. The minimum theoretical buckling loads for each beam type agree with the buckling modes that were observed in the experiments; that is that the C_0P_0 beam underwent Euler buckling while all of the others buckled in a torsional manner. Compared with the highest experimental data in each category, the theoretical values are off by 10.8% for the C_0P_0 case, 27.2% for the C_0P_X case, 13.3% for the C_2P_X case, and -2.4% for the C_1P_X case. The main source of error for these calculations is expected to be the accuracy of the C_t and C_w constants, as well as the fact that the impact of the periodic attachments were not considered.

Using Equation (2), along with k_z and k_w factors of 0.5, the theoretical critical moments can be seen compared to the experimental data in Figure 5b. For the C_0P_0 case in bending, instead of multiplying the critical moment by 3, the critical moment was calculated for each tape, using the moment of inertia for each of the 3 tape orientations. Compared with the highest experimental bending data in each category, the theoretical values are off by 27.2% for the C_0P_0 case, 19.4% for the C_2P_X case, and 15.1% for the C_1P_X case. Again, the main sources of error for these calculations are expected to be due to the C_t and C_w constants.

3. DYNAMIC TESTING

The objective of the dynamic testing is to measure the maximum tip deflections a beam undergoes during its use in a simple CDPM application at different accelerations and base inertia values.

3.1. Apparatus

In order to perform the dynamic tests, a dynamic testing apparatus was built, as shown in the sketch in Figure 6 and the picture in Figure 7a. A close-up of the end effector can be seen in Figure 7b. This apparatus allows horizontal rotation of a fixed-length beam about one end, driven by two beaded cables on

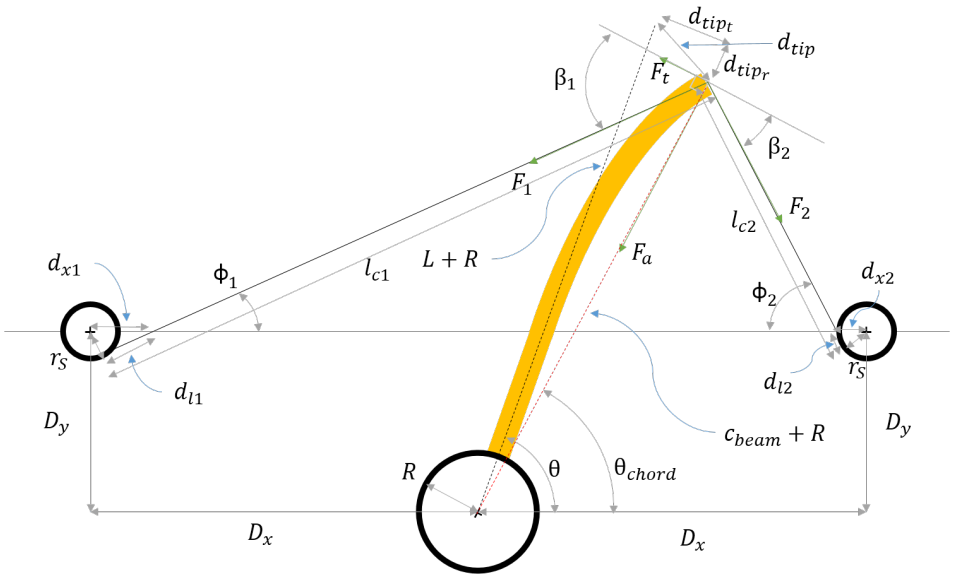

Fig. 6. Geometry of the dynamic apparatus with deflected beam.

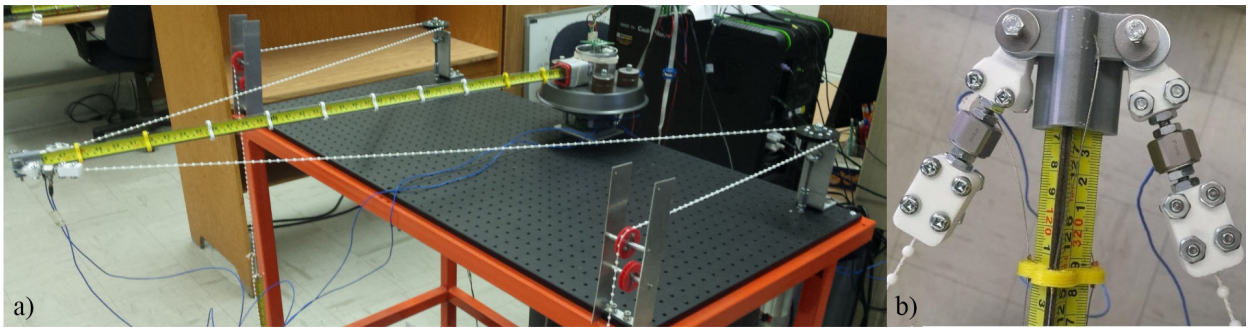

Fig. 7. a) Dynamic apparatus and b) end effector detail.

sprockets that are driven by motors. The test beams are inserted into a socket on a base hub, and on the other end another 3D printed piece allows the cables to connect to the beam. The base hub has four bolts where masses can be added to increase its inertia. The base hub is fixed to the optical breadboard table and includes two aligned bearings that allow it to rotate while a magnetic rotary encoder measures its angular displacement.

Each cable is driven by a motor mounted to the underside of the optic breadboard. Each motor drives a sprocket that allow the cables to be kept in tension. The end of each cable closest to the beam has a piezoelectric load cell to measure the cable forces, and they are connected to the cable and the end of the beam through 3D printed connectors and machine screws.

The magnetic rotary encoder, load cells, motor encoders, and current sensors are connected to an Arduino micro-controller which controls the speeds of the motors through two motor drivers. The Arduino runs PID controllers for each motor with desired speed profiles as inputs and the current speeds from the encoders as feedback. The PID control parameters were manually tuned to reduce the tracking error. The desired speed profiles were calculated for each acceleration value, as shown in the next section. As memory on the Arduino is limited, the data recording time was reduced to 0.3 s of the 1 s tests in order to maximize the sampling frequency (350 samples/second).

3.2. Kinematics and dynamics

The motion profile of the beam was described with a 5th order polynomial for the first and last t_1 seconds with constant velocity in between. For instance, for the first segment in the trajectory, the beam starts at rest, achieves maximum angular acceleration at $t = t_1/2$ and then reduces acceleration to zero until $t = t_1$ at which point the angular velocity is maximum. The boundary conditions for the last segment are symmetrical in time in order to have the beam finish the entire trajectory at rest. With $t_1 = 3\dot{\theta}_{max}/2\ddot{\theta}_{max}$, the profile for the acceleration and decelerations are described by

$$\theta = t^5 + \left(\frac{-4\ddot{\theta}_{max}^3}{27\dot{\theta}_{max}^2} - \frac{15\dot{\theta}_{max}}{4\ddot{\theta}_{max}}\right)t^4 + \left(\frac{4\ddot{\theta}_{max}^2}{9\dot{\theta}_{max}} + \frac{15\dot{\theta}_{max}^2}{4\ddot{\theta}_{max}^2}\right)t^3. \tag{3}$$

First, assuming that the beam is straight (that is that $\theta = \theta_{chord}$), the cable angles ϕ_2 and ϕ_1 can be determined as

$$\phi_1 = \tan^{-1}\left(\frac{(L+R)\sin\theta - D_y}{(L+R)\cos\theta + D_x + d_{x1}}\right) \quad \text{and} \quad \phi_2 = \tan^{-1}\left(\frac{(L+R)\sin\theta - D_y}{-(L+R)\cos\theta + D_x + d_{x2}}\right) \tag{4}$$

where θ is the beam angle, L is the beam length, R is the beam hub radius, D_x and D_y are the sprocket centre locations relative to the hub centre, and r_p is the cable sprocket radius.

The lengths d_x are $d_{x1} = r_p/\sin\phi_1$ and $d_{x2} = r_p/\sin\phi_2$ and, since they themselves functions of ϕ, the equations for ϕ and d_x must be solved iteratively.

The cable lengths l_{c_1} and l_{c_2} can be determined from

$$l_{c_i} = \left((L+R)\sin\theta - D_y - r_p\right)/\sin\phi_i \tag{5}$$

for $i = 1,2$, and differentiation gives the cable speeds from which the motor speeds can be determined.

The force angles β_1 and β_2 are defined as $\beta_1 = -\theta + \phi_1 + 90^\circ$ and $\beta_2 = \theta + \phi_2 - 90^\circ$.

With the angular acceleration profile known, the net tangential force, F_t, on the beam is determined as

$$F_t = \ddot{\theta} I_{total}/(L+R). \tag{6}$$

In terms of the geometry, the tangential and axial forces due to the cable forces F_1 and F_2 are

$$F_t = F_1\cos\beta_1 - F_2\cos\beta_2 \quad \text{and} \quad F_a = (F_1\sin\phi_1 + F_2\sin\phi_2)/\sin\theta. \tag{7}$$

Using these together, F_1 and F_2 can be determined by arbitrarily setting one and solving for the other. These were chosen such that they were similar in magnitude. With these forces, the torque on each motor can be determined and angular speed vs torque curves can be created and compared to the maximum specifications for the motors.

To measure the in-plane beam deflection d_{tip}, the location of the beam tip under the straight beam assumption must be compared to the deflected beam tip location. This deflected geometry includes the chord from the hub's axis of rotation to the deflected beam end, c_{beam}, and the angular displacement to this chord, θ_{chord}. The beam tip displacement, relative to its position as if it were a perfectly rigid beam, can be calculated as

$$d_{tip} = \sqrt{(L+R)^2 + (c_{beam}+R)^2 - 2(L+R)(c_{beam}+R)\cos(\theta - \theta_{chord})}. \tag{8}$$

The terms c_{beam} and θ_{chord} are defined as $c_{beam} = \sqrt{k_1^2 - k_2^2} - R$ and $\theta_{chord} = \tan^{-1}\left(\frac{k_1}{k_2}\right)$ where k_1 and k_2 are defined as $k_1 = \left(l_{c_1} - \frac{r_s}{\tan\phi_1}\right)\sin\phi_1 + D_y$ and $k_2 = \left(l_{c_1} - \frac{r_s}{\tan\phi_1}\right)\cos\phi_1 + \frac{r_s}{\sin\phi_1} - D_x$. The cable angles ϕ_1 and

ϕ_2 can be determined by solving the system of equations

$$\left(l_{c_1} - \frac{r_s}{\tan\phi_1}\right)\cos\phi_1 + \left(l_{c_2} - \frac{r_s}{\tan\phi_2}\right)\cos\phi_2 = 2D_x - \frac{r_s}{\sin\phi_1} - \frac{r_s}{\sin\phi_2} \tag{9}$$

$$\left(l_{c_1} - \frac{r_s}{\tan\phi_1}\right)\sin\phi_1 = \left(l_{c_2} - \frac{r_s}{\tan\phi_2}\right)\sin\phi_2, \tag{10}$$

which gives the two solutions

$$\phi_{1a} = -2\tan^{-1}\left(\frac{(4D_x r_s - k_3)(2D_x - l_{c_1} + l_{c_2})}{k_4(2D_x + l_{c_1} - l_{c_2})}\right), \quad \phi_{2a} = -2\tan^{-1}\left(\frac{4D_x r_s - k_3}{k_4}\right) \tag{11}$$

and

$$\phi_{1b} = 2\tan^{-1}\left(\frac{(4D_x r_s + k_3)(2D_x - l_{c_1} + l_{c_2})}{k_4(2D_x + l_{c_1} - l_{c_2})}\right), \quad \phi_{2b} = 2\tan^{-1}\left(\frac{4D_x r_s + k_3}{k_4}\right), \tag{12}$$

where $k_3 = \sqrt{-16D_x^4 + 8D_x^2 l_{c_1}^2 + 8D_x^2 l_{c_2}^2 + 16D_x^2 r_s^2 - l_{c_1}^4 + 2l_{c_1}^2 l_{c_2}^2 - l_{c_2}^4}$ and $k_4 = 4D_x^2 + 4D_x l_{c_2} - l_{c_1}^2 + l_{c_2}^2$.

These represent the assembly options for the cable to the sprockets; connecting on the top half or bottom half of the sprockets. In this case, the "*b*" solution is applicable.

3.3. Beam natural frequency

From the initial measurements of the dynamic testing, it was noticed that the beam's angular position was not as smooth as the planned path due to some form of oscillation. It was hypothesized that this was the beam itself vibrating, so the natural frequency of the beam was measured and then calculated theoretically, and these values were compared to the frequency observed in the test results.

In order to determine the oscillation frequency of the angular position data from the dynamic testing, a second order polynomial was fit to the data to act as a mean, and was then subtracted from the angular position data. A fast Fourier transform was then used to analyze the frequency components of this data, and the highest frequency component occurred at 10.06 Hz.

To determine the damped natural frequency of the beam in the dynamic jig, the two cables were tensioned by the motors to hold the far end of the beam in place, and a small impulse was imparted the the far end of the beam. The resulting angular position data was treated in the same manner as the previous data, and the highest frequency component occurred at 10.91 Hz.

The theoretical undamped natural frequency of the beam was also calculated as 10.66 Hz using $\frac{k_n}{2\pi}\sqrt{\frac{EIg}{wL^4}}$, approximating the beam as a simply supported beam since it is free to rotate at both ends [11]. In this equation, k_n is the coefficient for the first natural frequency of a simply supported beam with a distributed load w, and the distributed load w in N/m was calculated from the mass and length of the beam. This small frequency is due to the low stiffness of the beam.

3.4. Experimental design and results

The dynamic testing was carried out with 2 acceleration profiles and 3 base hub's inertia values, and a sample size of 15 tests per combination, resulting in 90 planned tests. The two profiles used in this testing were set such that the beam tip's acceleration would be 0.66 and 1 times the acceleration due to gravity (g = 9.81 m/s^2), using the profile parameters shown in Table 8. The three values for the base hub's inertia result from adding masses to the base as previously described. These values are summarized in Table 9.

The average results for the dynamic testing can be seen in Table 10. These results show small increases in the maximum dip deflection for changes in the base hub's inertia, and large changes between tests with the same inertia but different acceleration profiles. The acceleration appears to have a much larger impact on the beam's tip deflection than the inertia of the base.

Table 8. Acceleration profile parameters.

Profile	α_{max} (rad/s^2)	ω_{max} (rad/s)	Duration (s)	$\Delta\theta$ (rad)
0.66 g	5.97	0.32	1.00	0.294
1.00 g	9.05	0.96	1.00	0.807

Table 9. Inertia levels.

Base inertia (kg m^2)	Masses (g)	Inertia of masses (kg m^2)	Total inertia (kg m^2)
0.2202	0	0.0044	0.2245
0.2202	694	0.0081	0.2282
0.2202	1374	0.0113	0.2315

Table 10. Averages of dynamic test results.

Inertia (kg m^2)	d_{tip} at 0.66 g (mm)	d_{tip} at 1.00 g (mm)
0.225	47.89	56.75
0.228	48.06	60.55
0.231	48.20	60.98

4. CONCLUSIONS AND RECOMMENDATIONS

Of the 12 designs tested, beams with strip magnets and braces had the highest average loading capacities. Increasing the magnet width decreased the loading capacity in compression, while improving the loading capacity in bending. Increasing the beam's tape width was found to increase the loading capacities, while adding a spring core to the beam design was not found to significantly increase the loading capacities. The theoretical critical loads and moments were found to compare relatively well with the experimental results, as factors such as imperfections in the thin tapes and small amounts of eccentric loading would reduce the idealized theoretical critical capacities of the beams. In the dynamic testing, both increases in acceleration and inertia increased the tip displacement, but the impact of acceleration was much more significant.

The next step to address the overall problem outlined would be to design and build an actuator to turn this beam design into a linear actuator. Also, creating a model that determines the forces and displacements that an actuator would experience for any prescribed motion. If such a model was quick computationally, or a simplified model could be created, it could be used in real-time trajectory planning.

REFERENCES

1. Brown, G.W. "Patent US 4710819: Suspension system for supporting and conveying equipment, such as a camera", 1987.
2. Carretero, J.A. and Gosselin, C. "Wrench capabilities of cable-driven parallel mechanisms using wrench polytopes" In "Proc. of IFToMM Symposium on Mechanism Design for Robotics" , Montpelier, France, 2010.
3. Firmani, F., Zibil, A., Nokleby, S.B. and Podhorodeski, R.P. "Wrench capabilities of planar parallel manipulators. part I: Wrench polytopes and performance indices" *Robotica*, Vol. 26, No. 06, p. 791, April 2008.
4. Rauschenbach, H.S. "Solar cell array design handbook" Tech. Rep., NASA. Pages 196 - 203, October 1976. URL `https://ntrs.nasa.gov/search.jsp?R=19770007250`
5. Jaeger, F. and Siewert, A. "Patent US 980157: Portable extensible and retractable mast", 1910.
6. Watanabe, A., Ito, H., Hori, T. and Kawabata, N. "Patent US 8776451: Extendible structure", 2014.
7. Mathis, A. "High Packing Ratio Linear Actuator for use in Cable Driven Parallel Manipulators" University of New Brunswick, December 2018.
8. Terk, M. "Flexural-torsional buckling" Tech. Rep., 2005. URL `https://goo.gl/H6pkd2`
9. Inst. for Steel Development & Growth. *Introduction to Column Buckling*, 2018. URL `https://goo.gl/HrXA5r`
10. Ahnlén, M. and Westlund, J. *Lateral Torsional Buckling of I-beams: A Parametric Study of Elastic Critical Moments in Structural Design Software*. Master's thesis, 2013. URL `https://goo.gl/TpdqbF`
11. Beards, C. *Structural Vibration*. Elsevier Science, doi:10.1016/B978-0-340-64580-2.X5000-5, 1996.